DISCRETE AND CONTINUOUS
DYNAMICAL SYSTEMS SERIES S
Volume **4**, Number **6**, December **2011**

doi:10.3934/dcdss.2011.4.1413

pp. **1413–1428**

MULTIPLE STABLE STEADY STATES OF A REACTION-DIFFUSION MODEL ON ZEBRAFISH DORSAL-VENTRAL PATTERNING

Wenrui Hao, Jonathan D. Hauenstein, Bei Hu, Yuan Liu,
Andrew J. Sommese and Yong-Tao Zhang

Department of Mathematics, University of Notre Dame
Notre Dame, IN 46556, USA

Abstract. The reaction-diffusion system modeling the dorsal-ventral patterning during the zebrafish embryo development, developed in [Y.-T. Zhang, A.D. Lander, Q. Nie, Journal of Theoretical Biology, 248 (2007), 579–589] has multiple steady state solutions. In this paper, we describe the computation of seven steady state solutions found by discretizing the boundary value problem using a finite difference scheme and solving the resulting polynomial system using algorithms from numerical algebraic geometry. The stability of each of these steady state solutions is studied by mathematical analysis and numerical simulations via a time marching approach. The results of this paper show that three of the seven steady state solutions are stable and the location of the organizer of a zebrafish embryo determines which stable steady state pattern the multi-stability system converges to. Numerical simulations also show that the system is robust with respect to the change of the organizer size.

1. **Introduction.** The proper functioning of tissues and organs requires that each cell differentiates appropriately for its position. In many cases, the positional information that instructs cells about their prospective fates is conveyed by concentration gradients of morphogens bound to cellular receptors. Morphogens are signaling molecules that, when bound to receptors, assign different cell fates at different concentrations [10, 12]. Morphogen action is of special importance in understanding development, as it is a highly efficient way for a population of uncommitted cells in an embryo to create complex patterns of gene expression in space [6].

In [13], a nonlinear reaction-diffusion model on both three-dimensional and a simplified one-dimensional spatial domains was developed for computational analysis of BMP morphogen gradient formation in dorsal-ventral patterning of the zebrafish embryo. The model predicts that the dorsal organizer of the zebrafish embryo plays a key role in forming a stable non-homogeneous morphogen gradient, and the prediction agrees well with the existing biological experiments [7]. We briefly describe the model in the following paragraphs.

2000 *Mathematics Subject Classification.* Primary: 65H04, 65H20, 65M06, 65N06, 92B05.

Key words and phrases. Steady states, reaction-diffusion, polynomial systems, dorsal-ventral patterning.

W. Hao, J.D. Hauenstein and A.J. Sommese were supported by the Duncan Chair of the University of Notre Dame, NSF grant DMS-0410047, and NSF grant DMS-0712910. Y.-T. Zhang was supported by NSF grant DMS-0810413 and Oak Ridge Associated Universities (ORAU) Ralph E. Powe Junior Faculty Enhancement Award.

Consider the dorsal-ventral axis of the zebrafish embryo. The model simplifies it to a one-dimensional segment $0 \le x \le x_{max}$ with the dorsal organizer being located at the corner of the dorsal region, as shown in Figure 1.

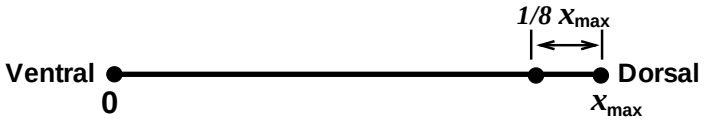

FIGURE 1. The simplified one dimensional geometry of wild type zebrafish embryo. The dorsal organizer is located at the end with the size $\frac{1}{8}$ of the whole embryo.

Let $[L]$ and $[LR]$ denote the concentration of the morphogen BMP and the concentration of BMP-receptor complexes (to which BMP signaling is assumed to be proportional), respectively. The concentration of the free molecule Chordin (an inhibitor of BMP) and the concentration of BMP-Chordin complex are denoted by $[C]$ and $[LC]$, respectively. Let R_0 denote the total receptor concentration and let D_L, D_C, and D_{LS} represent the three diffusion coefficients for BMP, Chordin, BMP-Chordin complexes, respectively. The values k_{on}, k_{off}, k_{deg}, j_{on}, j_{off}, and τ are the binding and degradation rates for BMP, Chordin, and their complexes. With this notation, the reaction-diffusion model that is formulated in [13] is as follows:

$$\begin{cases} \dfrac{\partial[L]}{\partial t} = D_L \dfrac{\partial^2[L]}{\partial x^2} - k_{on}[L](R_0 - [LR]) + k_{off}[LR] - j_{on}[L][C] + (j_{off} + \tau)[LC] + V_L; \\ \dfrac{\partial[LR]}{\partial t} = k_{on}[L](R_0 - [LR]) - (k_{off} + k_{deg})[LR]; \\ \dfrac{\partial[LC]}{\partial t} = D_{LS} \dfrac{\partial^2[LC]}{\partial x^2} + j_{on}[L][C] - (j_{off} + \tau)[LC]; \\ \dfrac{\partial[C]}{\partial t} = D_C \dfrac{\partial^2[C]}{\partial x^2} - j_{on}[L][C] + j_{off}[LC] + V_C, \end{cases} \tag{1.1}$$

where V_C and V_L are the production rates of molecules Chordin and BMP, respectively, defined by

$$V_C = V_{Cmin} + \frac{V_{Cmax} - V_{Cmin}}{1 + \gamma_C[LR]} + \begin{cases} V_{Corg}e^{-at}, & \text{if } x \in \Omega_O; \\ 0, & \text{otherwise.} \end{cases} \tag{1.2}$$

$$V_L = V_{Lmin} + \frac{V_{Lmax} - V_{Lmin}}{1 + \gamma_L[LR]^{-1}} + V_{Lmat}e^{-bt}. \tag{1.3}$$

The terms $V_{Corg}e^{-at}$ and $V_{Lmat}e^{-bt}$ represent the maternal production rates of Chordin and BMP [13]. Ω_O represents the organizer region which is a subset of the whole domain $[0, x_{max}]$. For the wild type zebrafish embryo, Ω_O is approximated by the interval $[\frac{7}{8}x_{max}, x_{max}]$ as shown in Figure 1.

The system (1.1) is subjected to the no-flux boundary conditions

$$\frac{\partial[L]}{\partial x} = \frac{\partial[LC]}{\partial x} = \frac{\partial[C]}{\partial x} = 0 \text{ for } x = 0, x_{max}. \tag{1.4}$$

Although no boundary condition is assumed for $[LR]$, the initial data for $[LR]$ does satisfy the no-flux boundary condition. Thus, by using the system (1.1), we also have

$$\frac{\partial [LR]}{\partial x} = 0 \text{ for } x = 0, x_{max}. \tag{1.5}$$

Parameter studies were performed in [13] with the following biological reasonable parameters

$$\begin{aligned}
&x_{max} = 0.088cm, \\
&D_L = D_{LS} = D_C = 8.5 \times 10^{-7} cm^2 s^{-1}, && k_{on} = 0.4\mu M^{-1} s^{-1}, \\
&R_0 = 3.0\mu M, && k_{off} = 4 \times 10^{-6} s^{-1}, \\
&j_{on} = 10\mu M^{-1} s^{-1}, && j_{off} = 1.0 \times 10^{-5} s^{-1}, \\
&\tau = 0.01 s^{-1}, && k_{deg} = 5.0 \times 10^{-4} s^{-1}, \\
&V_{Cmin} = 8.0 \times 10^{-4} \mu M s^{-1}, && V_{Cmax} = 8.0 \times 10^{-2} \mu M s^{-1}, \\
&V_{Corg} = 6.68 \times 10^{-1} \mu M s^{-1}, && \gamma_C = 10\mu M^{-1}, \\
&a = 0.0167 s^{-1}, && V_{Lmin} = 1.0 \times 10^{-5} \mu M s^{-1}, \\
&V_{Lmax} = 6.0 \times 10^{-3} \mu M s^{-1}, && \gamma_L = 10\mu M, \\
&V_{Lmat} = 5.01 \times 10^{-2} \mu M s^{-1}, && b = 0.0167 s^{-1},
\end{aligned} \tag{1.6}$$

a non-homogeneous spatial BMP morphogen gradient is formed. The high concentration region of BMP-receptor complex will develop into the ventral tissue of the zebrafish, and the low concentration region will become the dorsal part of the fish.

In this paper, we study multiple steady state solutions of the reaction-diffusion system (1.1). We obtain seven steady state solutions by numerically solving the corresponding boundary value problem using a combination of a finite difference discretization of the partial differential equations and numerical algebraic geometric methods for solving the resulting nonlinear algebraic system. The stability of each steady state solution is studied using mathematical analysis and numerical simulations via a time marching approach. We show that three of the seven steady state solutions are stable and the organizer of the zebrafish embryo plays an important role in the selection of the steady state pattern in this multi-stability system. These seven solutions were found by solving the nonlinear discretized system with nine spatial grid points. It is very possible that more solutions will appear with larger spatial grids.

To solve the time dependent system (1.1) numerically, we use a finite difference scheme [5]. The diffusion terms are approximated by the second order central difference. The adaptive Runge-Kutta-Fehlberg-2-3 method [9] is used for the temporal discretization. For the time-marching results presented in this paper, 321 spatial grid points $0 = x_0, x_1, \cdots, x_N = x_{max}$ and $N = 320$ are used. Convergence of the calculations is observed when the spatial meshes are refined. The overall accuracy of the time-marching computation is second order in space and third order in time.

2. **Multiple steady state solutions.** The steady state solutions of the system (1.1) satisfy the following boundary value problem:

$$\begin{cases} 0 = D_L \dfrac{\partial^2[L]}{\partial x^2} - k_{on}[L](R_0 - [LR]) + k_{off}[LR] - j_{on}[L][C] + (j_{off} + \tau)[LC] + V_L; \\ 0 = k_{on}[L](R_0 - [LR]) - (k_{off} + k_{deg})[LR]; \\ 0 = D_{LS} \dfrac{\partial^2[LC]}{\partial x^2} + j_{on}[L][C] - (j_{off} + \tau)[LC]; \\ 0 = D_C \dfrac{\partial^2[C]}{\partial x^2} - j_{on}[L][C] + j_{off}[LC] + V_C, \end{cases} \tag{2.1}$$

where

$$0 = x_{min} \le x \le x_{max} = 0.088cm, \tag{2.2}$$

$$V_C = V_{Cmin} + \frac{V_{Cmax} - V_{Cmin}}{1 + \gamma_C[LR]}, \tag{2.3}$$

and

$$V_L = V_{Lmin} + \frac{V_{Lmax} - V_{Lmin}}{1 + \gamma_L[LR]^{-1}}, \tag{2.4}$$

subjected to the no-flux boundary conditions

$$\frac{\partial[L]}{\partial x} = \frac{\partial[LC]}{\partial x} = \frac{\partial[C]}{\partial x} = 0. \tag{2.5}$$

The following section describes the computation of the seven steady state solutions we obtained for system (2.1).

2.1. **Computing multiple steady state solutions.** Steady state solutions to the boundary value problem (2.1) were found by discretizing and computing all solutions of the resulting system of equations using the software package Bertini [1, 2].

Observe that system (2.1) can be simplified by replacing the first equation with the sum of the first three equations and by replacing the last equation with the sum of the last two equations. Upon clearing denominators, we obtain the boundary value system

$$\begin{cases} 0 = ([LR] + \gamma_L)\left(D_L \dfrac{\partial^2[L]}{\partial x^2} - k_{deg}[LR] + D_{LS} \dfrac{\partial^2[LC]}{\partial x^2} + V_{Lmin}\right) + (V_{Lmax} - V_{Lmin})[LR]; \\ 0 = k_{on}[L](R_0 - [LR]) - (k_{off} + k_{deg})[LR]; \\ 0 = D_{LS} \dfrac{\partial^2[LC]}{\partial x^2} + j_{on}[L][C] - (j_{off} + \tau)[LC]; \\ 0 = (1 + \gamma_C[LR])\left(D_C \dfrac{\partial^2[C]}{\partial x^2} - \tau[LC] + V_{Cmin}\right) + V_{Cmax} - V_{Cmin}. \end{cases} \tag{2.6}$$

where $0 = x_{min} \leq x \leq x_{max} = 0.088cm$ with boundary conditions (2.5). This system is discretized using the second order central difference scheme for the interior conditions and left- and right-sided second order difference schemes for the boundary conditions with $\Delta x = \dfrac{x_{max} - x_{min}}{N}$, where $N \geq 3$. The boundary conditions for $[L]$ become

$$\begin{aligned} 3[L]_0 &= 4[L]_1 - [L]_2, \\ 3[L]_N &= 4[L]_{N-1} - [L]_{N-2}, \end{aligned}$$

with similar conditions for $[LC]$ and $[C]$.

Using the system (2.6), the boundary conditions for $[LR]$ are

$$\begin{aligned} k_{on}[L]_0(R_0 - [LR]_0) &= (k_{off} + k_{deg})[LR]_0, \\ k_{on}[L]_N(R_0 - [LR]_N) &= (k_{off} + k_{deg})[LR]_N. \end{aligned}$$

As suggested by (1.5), we could also utilize the no-flux boundary condition

$$\begin{aligned} 3[LR]_0 &= 4[LR]_1 - [LR]_2, \\ 3[LR]_N &= 4[LR]_{N-1} - [LR]_{N-2}. \end{aligned}$$

Either way, since (2.6) does not depend upon $\dfrac{\partial^2[LR]}{\partial x^2}$, $[LR]_0$ and $[LR]_N$ only appear in the boundary conditions for $[LR]$ in the discretized system. This means that they can be computed after the other values are known.

With these simplifications, the discretized polynomial system that we solved consisted of $4(N-1)$ quadratic polynomials in $4(N-1)$ variables. For $3 \leq N \leq 9$, we computed all solutions of this polynomial system using Bertini [1, 2]. Bertini is a software package in the field of numerical algebraic geometry that implements homotopy continuation based algorithms to numerically compute all solutions of polynomial systems over $\mathbb{C}$. For more information on homotopy continuation and the field of numerical algebraic geometry, see [8].

As suggested by (2.6), this polynomial system has an obvious linear product structure [11], one such linear decomposition, for $i = 1, \ldots, N$, is

$$\begin{aligned} \{1, [LR]_i\} &\times \{1, [LR]_i, [L]_{i-1}, [L]_i, [L]_{i+1}, [LC]_{i-1}, [LC]_i, [LC]_{i+1}\} \\ \{1, [LR]_i\} &\times \{1, [L]_i\} \\ \{1, [L]_i\} &\times \{1, [C]_i, [LC]_{i-1}, [LC]_i, [LC]_{i+1}\} \\ \{1, [LR]_i\} &\times \{1, [LC]_i, [C]_{i-1}, [C]_i, [C]_{i+1}\}. \end{aligned}$$

This linear product structure reduces the bound on the number of isolated solutions over $\mathbb{C}$ for the discretized system from its total degree bound of $2^{4(N-1)} = 16^{N-1}$ to 5^{N-1}. This bound is nearly sharp with our computations revealing that there are actually $5^{N-1} - 3^{N-1}$ solutions over $\mathbb{C}$.

For $3 \leq N \leq 9$, we used Bertini v1.1.1 with adaptive precision tracking [3, 4] to solve the discretized polynomial system. We ran Bertini on a cluster consisting of a manager that uses one core of a Xeon 5410 processor and up to 25 computing nodes, each containing two Xeon 5410 processors running 64-bit Linux, i.e., each node consists of 8 processing cores. Table 2.1 lists the linear product bound, the number of solutions over $\mathbb{C}$, the number of solutions over $\mathbb{R}$, the number of computing nodes utilized, and the time needed to compute all solutions of the discretized polynomial system.

N	lin. prod. bound	sol. over $\mathbb{C}$	sol. over $\mathbb{R}$	nodes	time
3	25	16	6	serial	2.7s
4	125	98	16	serial	14.4s
5	625	544	28	1	21.1s
6	3,125	2,882	184	5	51.6s
7	15,625	14,896	930	25	2m43s
8	78,125	75,938	3,720	25	35m2s
9	390,625	384,064	17,974	25	11h3m

TABLE 2.1. Summary of solving the discretized system for $3 \leq N \leq 9$

Using the real solutions, we constructed an approximate solution of the discretized system with 80 grid points by using a cubic spline. Each of these approximate solutions was refined and the resulting solutions that contained negative real values were discarded. This process yielded seven positive real solutions.

It is very possible that more than ten spatial grid points will lead to further solutions. At the rate of increase, eleven grid points ($N = 10$) would utilize upwards of ten days of computer time using the same computing resources used for ten grid points ($N = 9$). We did compute the symmetric solutions for the polynomial systems on spatial grids with 15 and 16 points, but found no additional solutions.

3. **Stability of the steady state solutions.**

The analysis of the steady state solutions utilized eigenvalue computations and numerical simulations via time marching. The eigenvalue analysis was computed using the non-dimensionalized system described in the next section.

3.1. **The non-dimensionalized system.**

To non-dimensionalize system (1.1), we introduced the following normalized quantities:

$$T = \frac{D}{x_{max}^2} t, \qquad X = \frac{x}{x_{max}}, \tag{3.1}$$

$$\{f_L, g_L, h_L, f_S, h_S, \tau_S\} = \frac{x_{max}^2}{D}\{k_{off}, k_{deg}, k_{on}R_0, j_{off}, j_{on}R_0, \tau\}, \tag{3.2}$$

$$\{A, B, C, S\} = \frac{1}{R_0}\{[L], [LR], [LC], [C]\}, \tag{3.3}$$

$$\begin{aligned}\{W_{Cmin}, W_{Cmax}, W_{Corg}, W_{Lmin}, W_{Lmax}, W_{Lmat}\} \\ = \frac{x_{max}^2}{DR_0}\{V_{Cmin}, V_{Cmax}, V_{Corg}, V_{Lmin}, V_{Lmax}, V_{Lmat}\},\end{aligned} \tag{3.4}$$

$$\{d_L, d_{LS}, d_C\} = \frac{1}{D}\{D_L, D_{LS}, D_C\}, \qquad \overline{\gamma_C} = \gamma_C R_0, \qquad \overline{\gamma_L} = \frac{\gamma_L}{R_0}, \tag{3.5}$$

where D is the maximum of D_L, D_{LS} and D_C in (1.6), namely

$$D = 8.5 \times 10^{-7} cm^2 s^{-1}.$$

With these normalized quantities, we rewrote the system (1.1) in the following dimensionless form:

$$\begin{cases} \dfrac{\partial A}{\partial T} = d_L \dfrac{\partial^2 A}{\partial X^2} - h_L A(1-B) + f_L B - h_S AS + (f_S + \tau_S)C + W_L; \\ \dfrac{\partial B}{\partial T} = h_L A(1-B) - (f_L + g_L)B; \\ \dfrac{\partial C}{\partial T} = d_{LS} \dfrac{\partial^2 C}{\partial X^2} + h_S AS - (f_S + \tau_S)C; \\ \dfrac{\partial S}{\partial T} = d_C \dfrac{\partial^2 S}{\partial X^2} - h_S AS + f_S C + W_C, \end{cases} \tag{3.6}$$

where

$$0 \le X \le 1$$

and

$$W_C = W_{Cmin} + \frac{W_{Cmax} - W_{Cmin}}{1 + \overline{\gamma_C} B} + \begin{cases} W_{Corg} e^{-PT}, & \text{if } X \ge \frac{7}{8}; \\ 0, & \text{otherwise.} \end{cases} \tag{3.7}$$

with

$$P = \frac{x_{max}^2}{D} a, \tag{3.8}$$

and

$$W_L = W_{Lmin} + \frac{W_{Lmax} - W_{Lmin}}{1 + \overline{\gamma_L} B^{-1}} + W_{Lmat} e^{-QT}, \tag{3.9}$$

with

$$Q = \frac{x_{max}^2}{D} b. \tag{3.10}$$

The non-dimensionalized parameters corresponding to those in (1.6) are:

$$\begin{array}{lll} d_L = d_{LS} = d_C = 1, & & h_L = 1.0924 \times 10^4, \\ f_L = 0.0364, & & h_S = 2.7310 \times 10^5, \\ f_S = 0.0910, & & \tau_S = 91.0326, \\ g_L = 4.5516, & & W_{Cmin} = 2.4275, \\ W_{Cmax} = 242.7536, & & W_{Corg} = 2.0270 \times 10^3, \\ \overline{\gamma_C} = 30, & & P = 152.0244, \\ W_{Lmin} = 0.0303, & & W_{Lmax} = 18.2065, \\ \overline{\gamma_L} = 3.3333, & W_{Lmat} = 152.0244, & Q = 152.0244. \end{array} \tag{3.11}$$

3.2. **Eigenvalue analysis of the steady state solutions.** The exponential terms in (3.7) and (3.9) correspond to the maternal production terms for the original system (1.1). These terms decay exponentially with $Q = P = 152.0244$, as shown in (3.11). Since we are considering the local stability of the steady state solutions, we drop the maternal production terms in the analysis of (3.6).

Assuming that

$$\begin{pmatrix} A \\ B \\ C \\ S \end{pmatrix} = \begin{pmatrix} A_0 \\ B_0 \\ C_0 \\ S_0 \end{pmatrix} + \varepsilon \begin{pmatrix} A_1 \\ B_1 \\ C_1 \\ S_1 \end{pmatrix} + O(\varepsilon^2),$$

the linearized system is

$$\begin{cases} A_{1T} = A_{1XX} - h_L A_1(1-B_0) + h_L A_0 B_1 + f_L B_1 - h_S A_1 S_0 - h_S A_0 S_1 + (f_S+\tau_S)C_1 \\ \qquad\qquad +B_1 \dfrac{(W_{L\max} - W_{L\min})\overline{\gamma_L}}{(\overline{\gamma_L}+B_0)^2}; \\ B_{1T} = h_L A_1(1-B_0) - h_L A_0 B_1 - (f_L+g_L)B_1; \\ C_{1T} = C_{1XX} + h_S A_1 S_0 + h_S A_0 S_1 - (f_S+\tau_S)C_1; \\ S_{1T} = S_{1XX} - h_S A_1 S_0 - h_S A_0 S_1 + f_S C_1 - B_1 \dfrac{(W_{C\max} - W_{C\min})\overline{\gamma_C}}{(1+\overline{\gamma_C}B_0)^2}. \end{cases} \tag{3.12}$$

For

$$Y(X,T) = \begin{pmatrix} A_1(X,T) \\ B_1(X,T) \\ C_1(X,T) \\ S_1(X,T) \end{pmatrix},$$

the system (3.12) can be written as

$$\frac{\partial Y}{\partial T} = \begin{pmatrix} 1 & & & \\ & 0 & & \\ & & 1 & \\ & & & 1 \end{pmatrix} Y_{XX} + M \cdot Y, \tag{3.13}$$

where

$$M = \begin{pmatrix} -h_L(1-B_0) - h_S S_0 & h_L A_0 + f_L + \dfrac{(W_{L\max} - W_{L\min})\overline{\gamma_L}}{(\overline{\gamma_L}+B_0)^2} & f_S+\tau_S & -h_S A_0 \\ h_L(1-B_0) & -h_L A_0 - (f_L+g_L) & 0 & 0 \\ h_S S_0 & 0 & -(f_S+\tau_S) & h_S A_0 \\ -h_S S_0 & -\dfrac{(W_{C\max} - W_{C\min})\overline{\gamma_C}}{(1+\overline{\gamma_C}B_0)^2} & f_S & -h_S A_0 \end{pmatrix}.$$

The seven steady state solutions consist of a constant solution and six non-constant solutions. The following establishes that the constant solution is unstable and three of the six non-constant solutions are also unstable.

I) Constant solution analysis.

For the constant solution, the vector (A_0, B_0, C_0, S_0) is constant as well as the matrix M. With the no-flux boundary conditions and separation of variables, we can always write

$$Y(X,T) = \sum_{n=0}^{\infty} \overrightarrow{b_n}(T)\ \cos(n\pi X),\ 0 \le X \le 1.$$

The system (3.13) yields

$$\frac{\partial}{\partial T}\overrightarrow{b_n}(T) = \left[\begin{pmatrix} -(n\pi)^2 & & & \\ & 0 & & \\ & & -(n\pi)^2 & \\ & & & -(n\pi)^2 \end{pmatrix} + M \right] \overrightarrow{b_n}(T),\ n = 0,1,2\cdots \tag{3.14}$$

Since $\{\cos(n\pi X)\}$ forms an orthogonal basis, the system (3.12) is asymptotically stable at the constant solution if and only if each system (3.14) is asymptotically stable for all $n = 0, 1, 2, \cdots$.

For each n, let

$$\mathcal{A}_n = \begin{pmatrix} -(n\pi)^2 & & & \\ & 0 & & \\ & & -(n\pi)^2 & \\ & & & -(n\pi)^2 \end{pmatrix} + M.$$

The ODE theory implies that the system (3.14) is stable if and only if each of the four eigenvalues for each $\mathcal{A}_n$ have negative real part. Evaluating M at the non-dimensionalized constant solution, both $\mathcal{A}_1$ and $\mathcal{A}_2$ have a real positive eigenvalue, namely, 0.3373 and 0.3634, respectively, yielding that the constant solution is not stable. □

II) General solution analysis

By separation of variables, we can write

$$Y(X, T) = e^{\lambda T} J(X). \tag{3.15}$$

The system (3.13) yields that

$$\mathcal{B}J = \begin{pmatrix} 1 & & & \\ & 0 & & \\ & & 1 & \\ & & & 1 \end{pmatrix} J_{XX} + M \cdot J = \lambda J$$

with the boundary conditions

$$(J_j)_X(0) = (J_j)_X(1) = 0 \text{ for } j = 1, 3, 4.$$

Although the boundary condition is not assumed for $j = 2$, the discussion earlier (see (1.5)) indicates that the no-flux boundary condition is also satisfied for $j = 2$.

It is clear from the explicit solution (3.15) that if the above eigenvalue problem admits an eigenvalue with positive real part, then the system is unstable.

Our expectation is that if μ is large enough, then the operator $-\mathcal{B} + \mu I$ is invertible and $(-\mathcal{B} + \mu I)^{-1}$ is a Fredholm operator. It follows that the only spectrum of this operator are eigenvalues. Note that $(-\mathcal{B} + \mu I)^{-1} h = \lambda h$, $h \neq 0$ if and only if $\lambda \neq 0$, $\mathcal{B}h = (\mu - \lambda^{-1})h, h \neq 0$. It follows that the only spectrum for $\mathcal{B}$ are the eigenvalues, and the stability depends on the real part of all eigenvalues being negative.

Let

$$J(X) = \begin{pmatrix} J_1(X) \\ J_2(X) \\ J_3(X) \\ J_4(X) \end{pmatrix}$$

and

$$M(X) = (m_{ij}(X))_{1 \le i,j \le 4},$$

we calculate the numerical solutions of the eigenvalue problem. With grid points $0 = X_0, X_1, ..., X_{N-1}, X_N = 1$, here, $N = 320$ in our computation, the boundary conditions yield

$$\begin{aligned} J(X_0) &= \frac{4J(X_1) - J(X_2)}{3}, \\ J(X_N) &= \frac{4J(X_{N-1}) - J(X_{N-2})}{3}. \end{aligned} \tag{3.16}$$

Then the eigenvalue problem is discretized as

$$\begin{pmatrix} N^2 & & & \\ & 0 & & \\ & & N^2 & \\ & & & N^2 \end{pmatrix} (J(X_{k+1}) - 2J(X_k) + J(X_{k-1})) + M(X_k) \cdot J(X_k) = \lambda J(X_k), \tag{3.17}$$

or, more specifically,

$$\begin{aligned} &N^2(J_1(X_{k+1}) - 2J_1(X_k) + J_1(X_{k-1})) + \sum_{j=1}^{4} m_{1j}(X_k) J_j(X_k) = \lambda J_1(X_k), 1 \le k \le N-1; \\ &\sum_{j=1}^{4} m_{2j}(X_k) J_j(X_k) = \lambda J_2(X_k), \qquad 0 \le k \le N; \\ &N^2(J_3(X_{k+1}) - 2J_3(X_k) + J_3(X_{k-1})) + \sum_{j=1}^{4} m_{3j}(X_k) J_j(X_k) = \lambda J_3(X_k), 1 \le k \le N-1; \\ &N^2(J_4(X_{k+1}) - 2J_4(X_k) + J_4(X_{k-1})) + \sum_{j=1}^{4} m_{4j}(X_k) J_j(X_k) = \lambda J_4(X_k), 1 \le k \le N-1. \end{aligned} \tag{3.18}$$

Letting

$$V = \begin{pmatrix} J_2(X_0) \\ J_1(X_1) \\ J_2(X_1) \\ J_3(X_1) \\ J_4(X_1) \\ \cdots \\ J_1(X_{N-1}) \\ J_2(X_{N-1}) \\ J_3(X_{N-1}) \\ J_4(X_{N-1}) \\ J_2(X_N) \end{pmatrix},$$

and denoting the coefficients matrix of (3.18) by G, we can rewrite (3.18) in the matrix form

$$G \cdot V = \lambda \cdot V. \tag{3.19}$$

So finally, the eigenvalue problem reduces to calculating the eigenvalues of the matrix G.

For each of the seven steady state solutions on 320 grid points, we computed the matrix G and its eigenvalues, and obtained the following results:

Solutions 1 and 2: These two solutions have the same eigenvalues. All the eigenvalues have negative real parts as shown in Figure 2. The eigenvalue of each solution with maximum real part is $-0.1455 \pm 1.47146i$.

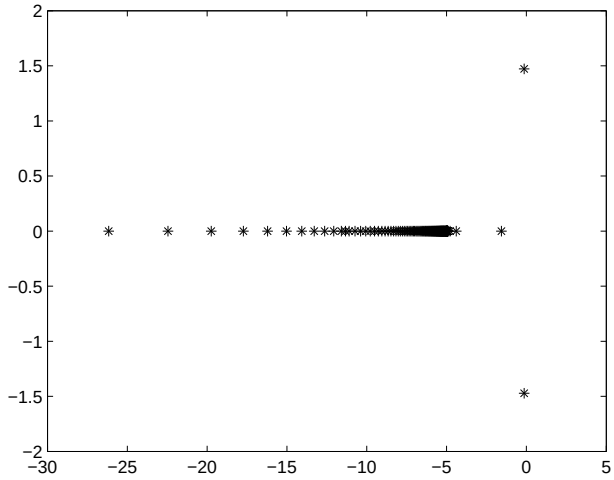

FIGURE 2. The distribution of the eigenvalues on the complex plane for solutions 1 and 2

Solution 3 (constant solution): To verify our computations, we recomputed the eigenvalues for the constant solution using this discretization and verified the two positive eigenvalues of 0.3373 and 0.3634.

Solution 4: All the eigenvalues have negative real parts and are displayed in Figure 3. The eigenvalue with maximum real part is -0.2826.

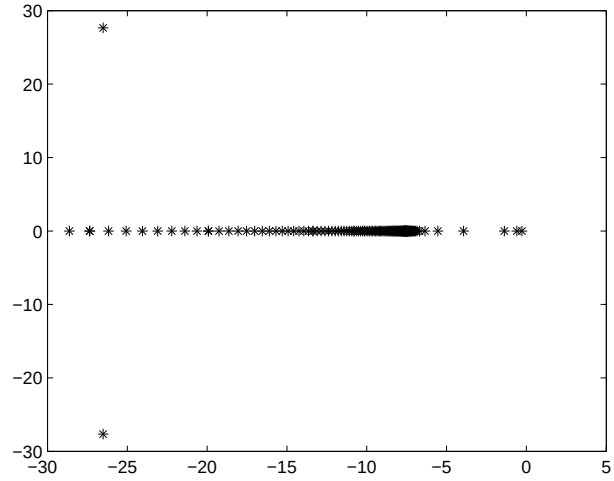

FIGURE 3. The distribution of the eigenvalues on the complex plane for solution 4

Solution 5: This solution has a positive eigenvalue, namely 1.2812.

Solutions 6 and 7: These solutions have a positive eigenvalue, namely 0.4351.

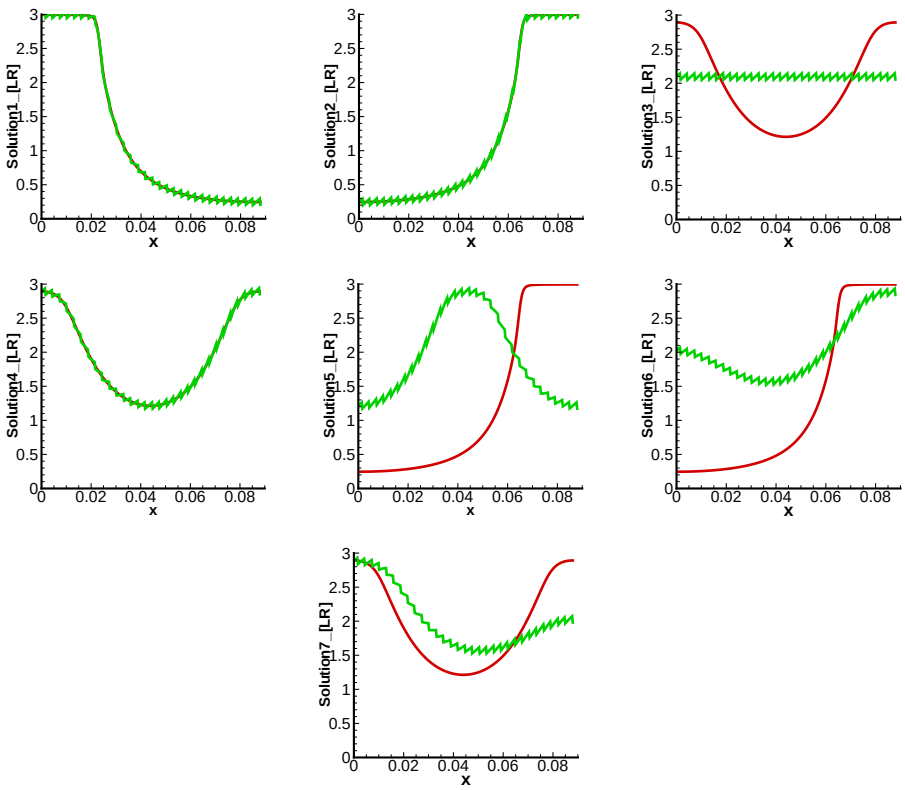

FIGURE 4. The steady state solutions by time-marching the system (1.1) without the maternal production terms. The unit for x of the horizontal axis: cm; the unit for [LR] of the vertical axis: μM. Initial conditions are the boundary value problem solutions by the numerical algebraic geometry method, with random perturbations. The perturbation size is $[-0.05, 0.05]$. Green oscillatory lines: the initial conditions. Red lines: the steady states by time-marching, at time $t = 100$ hours. Top three pictures from the left to the right are for: the solution 1, the solution 2 and the solution 3; middle three pictures from the left to the right are for: the solution 4, the solution 5 and the solution 6; bottom picture is for: the solution 7.

In summary, the solutions, denoted as solutions 1, 2, and 4, have eigenvalues which have negative real parts yielding that they are stable. □

3.3. **Numerical verification.** By time marching the system (1.1) without the maternal production terms, we numerically verified the local stability of the seven steady state solutions. This was accomplished by using a random perturbation of a solution of the boundary value problem as the initial condition as computing the steady state solution.

We first perturbed each steady state solution of size $[-0.05, 0.05]$. The results, summarized in Figure 4, demonstrate that the four solutions which have an eigenvalue with positive real part, as computed in Section 3.2, do not converge back to

the un-perturbed steady state solution. They converge to one of the stable steady state solutions.

The three solutions which only have eigenvalues with negative real parts converge back to the un-perturbed steady state solution. By changing the size of the perturbation, we computed a local stability region for the three stable steady state solutions. In our tests, both **solutions 1** and **2** converged to itself if the perturbation size was $[-0.23, 0.23]$ and **solution 4** converged to itself if the perturbation size was $[-1.52, 1.52]$.

Hence we numerically verified that 3 of these 7 steady state solutions are locally stable, while the other 4 are unstable.

4. **Role of the organizer.** The non-homogeneous [LR] concentration of a stable steady state solution of the system will determine the dorsal-ventral regions of a zebrafish embryo. Since this system has multiple stable steady state solutions as what we have found and analyzed in the previous sections, an interesting question will be "what will the dorsal-ventral regions be for a specific zebrafish embryo?" or "which stable steady state will the system converge to for a specific development process?". In this section, we numerically solved the full time-dependent system (1.1) with the maternal production terms, and we vary the size and location of the organizer (i.e., vary Ω_O to be different intervals) to study the effects of the organizer. Via numerical simulations, we find that the location of the organizer plays an important role in the selection of the steady state pattern in this multistability system.

All molecules have zero initial concentrations in the simulations. We used 321 spatial grid points and the grid size is $\Delta x = x_{max}/320$.

4.1. **Organizer location.** The numerical simulation results shown in Figure 5 demonstrate that the location of the organizer determines which stable steady state the system will converge to. When the organizer is located close to the right end of the interval, the time-marching solution converges to the stable steady state solution 1, and, if the organizer is located close to the left end of the interval, the time-marching solution converges to the stable steady state solution 2. The time-marching solution converges to the stable steady state solution 4 if the organizer location is close to the middle of the interval.

4.2. **Organizer size.** The system is robust with respect to the change of the organizer size, which is consistent with the biological experiments [7]. In our simulations, we assume that the organizer is located at the right end, just as the wild type case [13]. We vary the organizer size from $\frac{1}{2}$ of the whole domain to only $\frac{1}{320}$ of the domain, and study the effect on the steady state pattern. The results of these simulations are summarized in Figure 6 and show that the steady state solution is independent of the organizer size.

5. **Conclusion.** In this paper, we study the multiple stable steady states for a reaction-diffusion system modeling the dorsal-ventral patterning during zebrafish embryo development. First, we combine a finite difference discretization of the differential equations and numerical algebraic geometric methods to solve the boundary value problem at the steady state of the system, and obtain seven steady state solutions. Then we analyze the stability of these seven solutions using both the eigenvalue analysis and numerical time marching approach, and find that three of these seven steady state solutions are stable. Since this system has multiple stable

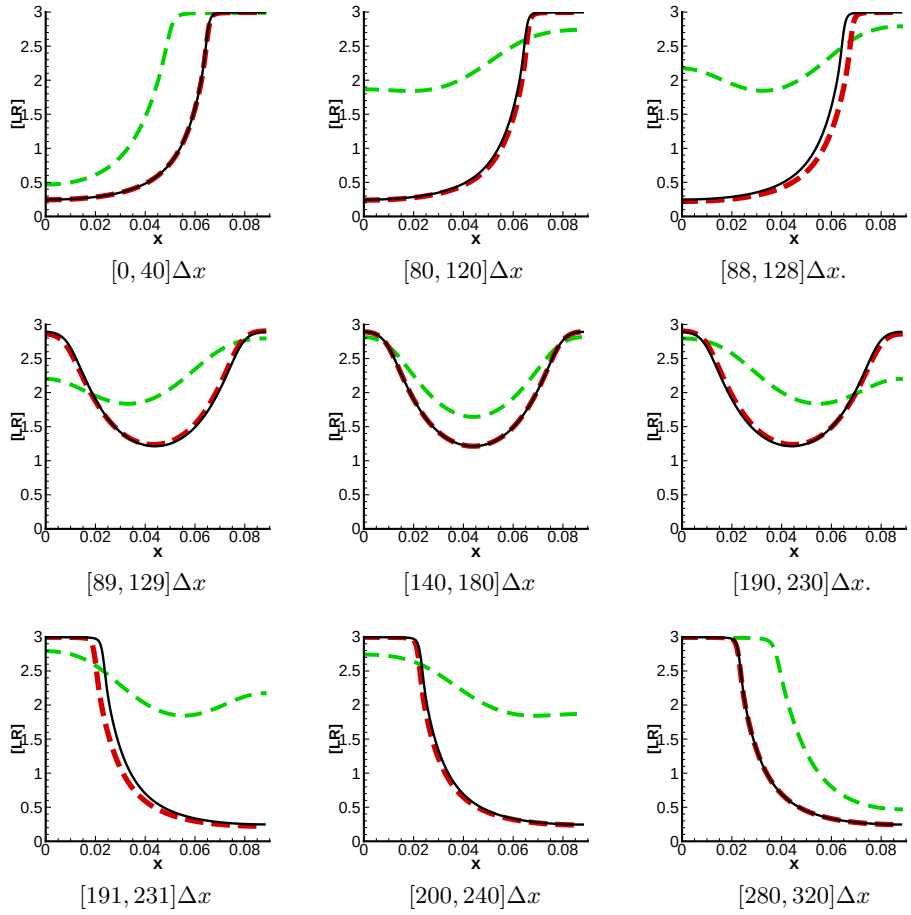

FIGURE 5. The evolution process of [LR] to steady states, with different organizer locations. The organizer region Ω_O is presented right below each graph. The size of the organizer is fixed as $\frac{1}{8}x_{max}$ here. The spatial grid size $\Delta x = x_{max}/320$. The unit for x of the horizontal axis: cm; the unit for [LR] of the vertical axis: μM. In each graph, Green dashed: the concentration of [LR] when $t = 3.5$ hours; Red dashed: the concentration of [LR] when $t = 50$ hours; Black solid: the concentration of [LR] when $t = 100$ hours.

steady state solutions which are biological meaningful, we investigate the question "which stable steady state will the system converge to for a specific development process?" and find that the location of the organizer determines which stable steady state the system will converge to.

The polynomial numerical algebraic geometric method is a powerful approach which enables us to find as many steady state solutions as we can, and gives guidance on finding multiple stable and biological meaningful steady state solutions. Time-marching approach is a powerful tool but (a) since starting from a specific initial state, each time-marching approach may reach at most one stable steady state solution, and (b) unstable steady solution cannot be found by time-marching

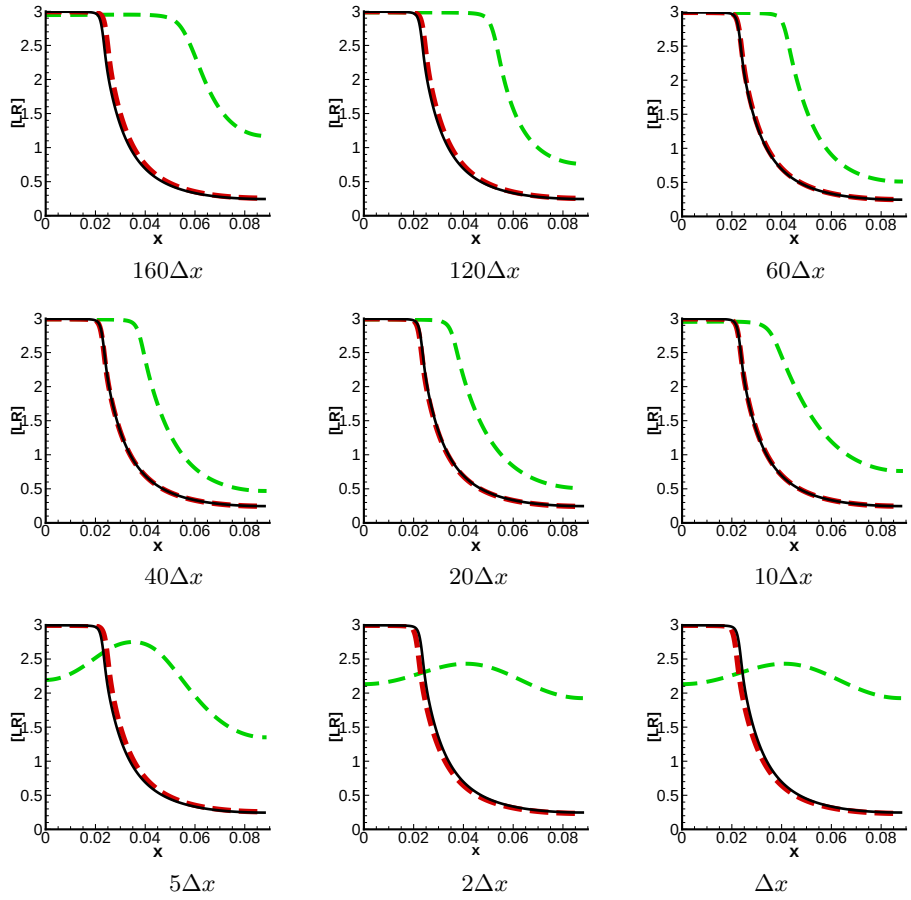

FIGURE 6. The evolution process of [LR] to a steady state, with different organizer sizes. The organizer region is located at the right end, with different sizes. The sizes of the organizer are listed right below each figure. The spatial grid size $\Delta x = x_{max}/320$. The unit for x of the horizontal axis: cm; the unit for [LR] of the vertical axis: μM. In each graph, Green dashed: the concentration of [LR] when $t = 3.5$ hours; Red dashed: the concentration of [LR] when $t = 50$ hours; Black solid: the concentration of [LR] when $t = 100$ hours.

approach. Polynomial treatment provides the steady state solutions directly and then the stability can be verified by either time-marching or eigenvalue method.

In this model (1.1), the effects of organizer decay exponentially to zero along with time evolution. Hence the shapes of these three steady state solutions are independent of the organizer. But as what we show in the section 4, the organizer which generates a non-homogeneous production rate for Chordin can provide a non-homogeneous initial state for the system, and determines which stable steady state the system converges to for this multiple steady states system.

REFERENCES

[1] D. J. Bates, J. D. Hauenstein, A. J. Sommese and C. W. Wampler, "Bertini: Software for Numerical Algebraic Geometry," Available at http://www.nd.edu/$\sim$sommese/bertini.

[2] D. J. Bates, J. D. Hauenstein, A. J. Sommese and C. W. Wampler, II, *Software for numerical algebraic geometry: A paradigm and progress towards its implementation*, in "Software for Algebraic Geometry," volume **148** of IMA Vol. Math. Appl., 1–14. Springer, New York, 2008.

[3] D. J. Bates, J. D. Hauenstein, A. J. Sommese and C. W. Wampler, *Adaptive multiprecision path tracking*, SIAM J. Numer. Anal., **46** (2008), 722–746.

[4] D. J. Bates, J. D. Hauenstein, A. J. Sommese and C. W. Wampler, *Stepsize control for adaptive multiprecision path tracking*, in "Interactions of Classical and Numerical Algebraic Geometry" (eds. D. Bates, G. Besana, S. Di Rocco and C. Wampler), Contemporary Mathematics, **496** (2009), 21–31.

[5] B. Gustafsson, H.-O. Kreiss and J. Oliger, "Time Dependent Problems and Difference Methods," Wiley, New York, 1995.

[6] A. D. Lander, *Morpheus unbound: Reimagining the Morphogen gradient*, Cell, **128** (2007), 245–256.

[7] L. Saude, K. Woolley, P. Martin, W. Driever and D. L. Stemple, *Axis-inducing activities and cell fates of the zebrafish organizer*, Development, **127** (2000), 3407–3417.

[8] A. J. Sommese and C. W. Wampler, II, "The Numerical Solution of Systems of Polynomials Arising in Engineering and Science," World Scientific Publishing Co. Pte. Ltd., Hackensack, NJ, 2005.

[9] J. Stoer and R. Bulirsch, "Introduction to Numerical Analysis," Springer-Verlag, New York, 1993.

[10] A. A. Teleman, M. Strigini and S. M. Cohen, *Shaping morphogen gradients*, Cell, **105** (2001), 559–562.

[11] J. Verschelde and R. Cools, *Symbolic homotopy construction*, Appl. Algebra Engrg. Comm. Comput., **4** (1993), 169–183.

[12] L. Wolpert, R. Beddington, J. Brockets, T. Jessel, P. Lawrence and E. Meyerowitz, "Principles of Development," Oxford University, 2002.

[13] Y.-T. Zhang, A. Lander and Q. Nie, *Computational analysis of BMP gradients in dorsal-ventral patterning of the zebrafish embryo*, Journal of Theoretical Biology, **248** (2007), 579–589.

Received May 2009; revised September 2009.

E-mail address: whao@nd.edu
E-mail address: jhauenst@math.tamu.edu;(www.math.tamu.edu/∼jhauenst)
E-mail address: b1hu@nd.edu
E-mail address: yliu7@nd.edu
E-mail address: sommese@nd.edu;(www.nd.edu/∼sommese)
E-mail address: yzhang10@nd.edu